Oxygen–metal bonding in Ti-bearing compounds from O 1s spectra and *ab initio* full multiple-scattering calculations

Ziyu Wu,[a,b,c*] E. Paris,[c] F. Langenhorst[d] and F. Seifert[d]

[a]Beijing Synchrotron Radiation Facility, Institute of High Energy Physics, Chinese Academy of Sciences, PO Box 918, Beijing 100039, People's Republic of China, [b]INFN-Laboratori Nazionali di Frascati, PO Box 13, I-00044 Frascati, Italy, [c]Dipartimento di Scienze della Terra and INFM, Università di Camerino, I-62032 Camerino, Italy, and [d]Bayerisches Geoinstitut, Universität Bayreuth, D-95440 Bayreuth, Germany.
E-mail: wuzy@ihep.ac.cn

The O K-edge spectra of a series of Ti-bearing compounds with Ti in different structural and chemical environments have been measured using electron energy-loss spectroscopy and analyzed using *ab initio* full multiple-scattering (MS) calculations. The near-edge structures arise mainly from covalency by direct and/or indirect interaction between O and metal atoms and between O and Si atoms. The coordination number of the cation and the site symmetry also influence the spectral shape and structures. Using different size clusters around the excited atom in the full MS simulation, it is possible to interpret and assign the features present in the spectra of each compound to its specific atomic arrangement and electronic structure.

1. Introduction

Bonding in silicates is characterized by a strong covalent component in the Si—O bond (Gibbs *et al.*, 1994), *i.e.* a reduced charge on the Si atoms, compared with that expected in an ionic model, caused by a charge transfer from O^{2-} to silicon and to some extent also to other cations (de Groot *et al.*, 1989; Soriano *et al.*, 1993; Wu *et al.*, 1998). The O $2p$ orbitals thus have an empty antibonding part owing to hybridization with these empty atomic orbitals. This can be investigated by O K-edge XANES (X-ray absorption near-edge structure) and/or ELNES (electron energy loss near-edge structure) experiments, as it involves, according to the dipole selection rule, a $1s$–$2p$ electronic transition. The shape of the O K-edge spectra have been shown to be particularly sensitive to the nature of the transition metal contained (de Groot *et al.*, 1989; Kurata *et al.*, 1993; van Aken *et al.*, 1998*a*). So far, XANES has mostly been used to elucidate the electronic and atomic structures of transition metals by measuring their L-edges (Garvie & Craven, 1994; Garvie & Buseck, 1998; van Aken *et al.*, 1998*b*), principally in fairly simple structures. For the O K-edge spectra that are of interest here, technical difficulties in measuring XANES spectra existed for a long time because of the low energy involved (*ca.* 530 eV). Moreover, the interpretation of O K-edge spectra remains difficult for the large number of O sites present in complex systems, which limits the investigation to quite simple binary oxides (Wu, Ouvrard *et al.*, 1997; van Aken *et al.*, 1999; de Jollet *et al.*, 1997; Yoshiya *et al.*, 1999; Soldatov *et al.*, 2000).

The technical problems with the acquisition of O K-edge spectra have been overcome with the development of new dedicated monochromators for low X-ray energies and with the refinement of the ELNES method (Egerton, 1996), which is particularly suited for this energy range. X-ray absorption spectroscopy (XAS) and electron energy loss spectroscopy (EELS) are based on the same fundamental physical process. The incident X-rays in XAS or the incident fast electrons in EELS excite core electrons to empty states above the Fermi level. When we study the K-edge of oxygen, the initial state is $1s$, and thus we probe final oxygen p states according to the dipole selection rule $\Delta l = \pm 1$. These two techniques also have several complementary features: XAS has a better energy resolution and EELS a much better spacial resolution Furthermore, full multiple-scattering (MS) calculations now allow the interpretation of XANES/ELNES spectra even in structurally complex materials (Wu, Marcelli *et al.*, 1997; Cabaret *et al.*, 1998). Indeed, the low-energy part of an absorption spectrum is very sensitive to the geometrical arrangement of the environment surrounding the selected atom, because the photoelectron emitted by the photoabsorber undergoes multiple scattering events and interacts with many other atoms in its environment. It therefore may simultaneously probe the geometry and electronic structure of an n-particle distribution function.

In this paper, we present a series of ELNES spectra at the O K-edge in several Ti-bearing natural and synthetic compounds: Ba_2TiO_4, $Ba_2TiSi_2O_8$ (synthetic fresnoite), $CaTiSiO_5$ (natural titanite), and perovskites $XTiO_3$ with X = Ca, Sr and Ba. This suite of samples allows us to probe the oxygen–metal bond (where the metal is mostly titanium) and to investigate how the bond is affected by the first and second neighbors and by the variable coordination geometry. In fact, these compounds have been chosen for this study because they represent a set of standards for titanium in different coordination environments, and their characterization, both at oxygen and titanium edges, is essential for the study of site location of trace titanium in minerals and glasses or for the identification of cation ordering and clustering. With the help of full MS calculations, using increasing cluster sizes around the excited O atom, we demonstrate that the specific atomic arrangement and the electronic structure of each compound can be described in terms of the position, shape and intensity of the characteristic features of the ELNES spectra.

2. Calculations

Calculations were based on the one-electron full multiple-scattering (MS) theory (Stöhr, 1988; Durham, 1988; Lee & Pendry, 1975; Natoli & Benfatto, 1986; Natoli *et al.*, 1986, 1990) using the extended *CONTINUUM* code developed by Natoli *et al.* (1980). We have used the Mattheiss (1964) prescription to construct the cluster electronic density and the Coulomb part of the potential by superposition of neutral atomic charge densities obtained from the Clementi–Roetti tables (Clementi & Roetti, 1974). In order to simulate the charge relaxation around the core hole in the photoabsorber of atomic number Z we have used the screened $Z + 1$ approximation (final-state rule) (Lee & Beni, 1977), which takes the orbitals of the $Z + 1$ atom and constructs the final-state charge density using the excited configuration of the photoabsorber with the core electron promoted to a valence orbital.

From practical experience of edge-feature simulations for these systems, we have taken a complex X_α as the exchange-correlation part of the potential, *i.e.* taking the X_α potential as the real part and the imaginary part of the energy- and position-dependent complex Hedin–Lundquist (H–L) self energy $\Sigma(\mathbf{r}, E)$ as the imaginary part (Penn, 1987), which gives the amplitude attenuation of the excited photoelectronic wave due to extrinsic inelastic losses and automatically takes into account the photoelectron mean free path in the

excited final state. The use of the X_α exchange-correlation potential is not a limitation, since at low energies (around 30 eV above the onset of the absorption, the energy region of interest) this potential and the real part of the Hedin–Lundquist potential nearly coincide if the constant X_α is appropriately chosen. Convergence of the calculated spectra was reached for cluster sizes of *ca.* 6 Å radius. The calculated spectra are further convoluted with a Lorentzian function with a full width $\Gamma_h = \sim 0.2$ eV to account for the core-hole lifetime and an experimental resolution $\Gamma_{exp} = \sim 0.8$ eV. We have chosen the muffin-tin radii according to the criterion of Norman (1974) and allowed a 10% overlap between contiguous spheres to simulate the atomic bond. The calculated spectra have been aligned in terms of the muffin-tin potential of clusters.

3. Experimental methods

$Ba_2TiSi_2O_8$ was synthesized in air using as a starting material a mixture of oxides in stoichiometric proportions (TiO_2, SiO_2 and BaO, which was obtained after decarbonatation of $BaCO_3$ at 1173 K). The mixture, after homogenization achieved by grinding it in an agate mortar, was heated in air at 1573 K for 13 h, then at 1373 K for 6 h, and quenched. Ba_2TiO_4 was obtained using an oxide mixture composed of TiO_2 and BaO (obtained after decarbonatation of $BaCO_3$). The synthesis was carried out in air, heating the mixture at 1473 K for 24 h and then cooling slowly to 473 K. The synthesis products were checked using X-ray diffraction. We used a natural sample of titanite ($CaTiSiO_5$) (mineral collection, University of Camerino), and the perovskite samples ($XTiO_3$) were commercially available materials.

For transmission electron microscope (TEM) studies, the samples were crushed in a mortar, suspended in alcohol and then deposited on 3 mm Cu TEM grids coated with a holey amorphous carbon film. O K-edge ELNES spectra were collected with a Gatan PEELS 666 parallel electron spectrometer attached to a PHILIPS CM20-FEG (field emission gun) TEM operating at 200 kV.

The energy resolution of the Schottky field-emitter, defined as the full width at half-maximum height of the zero-loss peak, was between 0.75 and 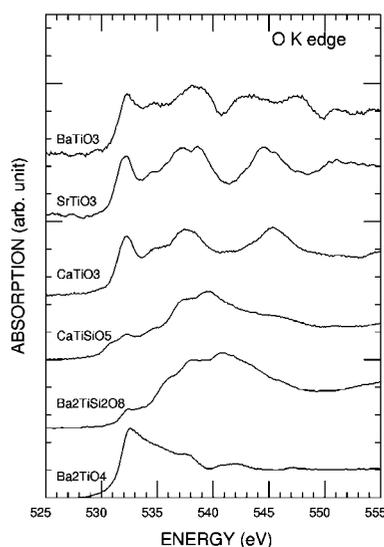0.8 eV. All spectra were collected in the diffraction mode with an illumination $a = 8.0$ mrad, collection semiangles $b = 1.45$ mrad and a 2 mm PEELS aperture. The measurements of the O K-edge spectra were performed with an energy dispersion of 0.1 eV per channel and an integration time $t = 10$–20 s per readout. Data reduction of these spectra included the correction for the dark current, the channel-to-channel gain variation, the subtraction of an inverse power law background and the removal of plural scattering contributions by the Fourier-ratio deconvolution technique. The energy scale of the EELS spectra was calibrated by measuring simultaneously the C K-edge of the amorphous carbon foil and the Ti L- and O K-edges of samples with an energy dispersion of 0.3 eV per channel. The $\pi*$ peak of the C K-edge at 285 eV served as a reference for calibration. This procedure allows one to check that the energy scales of the O K-edge spectra for the different samples are not shifted relative to each other. The spectra of the different samples are therefore directly comparable. However, because of uncertainties in the energy dispersion of the spectrometer, the absolute energy values may present a systematic error, estimated to be less than 0.5 eV.

4. Results and discussion

Fig. 1 shows the experimental O K-edge ELNES spectra of Ti-bearing compounds $Ba_2Ti^{[4]}O_4$, $BaTi_2^{[5]}Si_2O_8$ (fresnoite), $CaTi^{[6]}SiO_5$ (titanite), and perovskites $XTi^{[6]}O_3$ with X = Ca, Sr and Ba. To our knowledge, the first three spectra have not yet been published, and the O K-edges of the perovskites are in good agreement with previous published works (van Aken *et al.*, 1998a; Brydson *et al.*, 1992; de Groot *et al.*, 1993).

Fig. 1 clearly shows the similarities between the $XTiO_3$ spectra and the distinct differences with the spectra of the other compounds. Fig. 2 shows the MS theoretical calculation of the total O K-edge spectra for four compounds. In the following, we will analyze the spectra in detail in terms of site symmetry and atomic environment. Lattice constants and structural parameters employed in the calculations are available on request.

4.1. $Ba_2Ti^{[4]}O_4$

Barium orthotitanate, $Ba_2Ti^{[4]}O_4$, is one of the few compounds in which Ti is coordinated with four O atoms and has a monoclinic
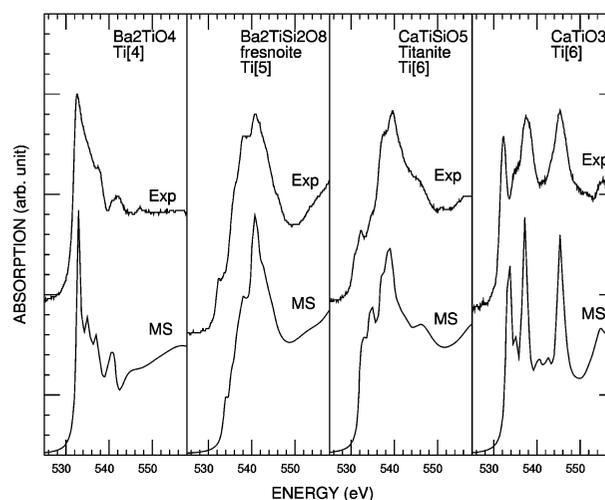

Figure 1
Experimental ELNES spectra at the O K-edge for $Ba_2Ti^{[4]}O_4$, $Ba_2Ti^{[5]}Si_2O_8$ (fresnoite), $CaTi^{[6]}SiO_5$ (titanite), and perovskites $XTi^{[6]}O_3$ with X = Ca, Sr, and Ba.

Figure 2
Comparison of the MS-calculated O K-edge spectra with experimental data: from left to right, Ba_2TiO_4, fresnoite ($Ba_2TiSi_2O_8$), titanite ($CaTiSiO_5$) and perovskite $CaTiO_3$.

symmetry in space group $P2_1/n$. Each unit cell contains four isolated TiO$_4$ tetrahedra linked by Ba atoms (Wu & Brown, 1973). Ti—O distances range from 1.766 Å for O1 to 1.836 Å for O4, which results in O1 being bonded to only three Ba atoms and one Ti atom while each of the other O atoms are bonded to four Ba atoms and one Ti atom.

In Fig. 3, we present calculations of the O K-edge ELNES spectra for four individual O-atom sites using different atomic clusters containing increasing coordination shells. The final clusters correspond to spheres of 6 Å radius around the photoabsorber atom with O taken as the center of the cluster; a larger 7 Å-radius cluster calculation does not show any significant difference. The left panel shows the calculated spectra as a function of cluster size obtained by summing the contributions of four individual O-atom sites in the proportion 1:1:1:1. The two-shell cluster already gives rise to a definite strong pre-edge peak A associated with transitions to anti-bonding O 2p states hybridized with the Ti 3d and/or Ba 5d orbitals, mainly localized at the metal sites. In the language of molecular orbital theory, peak D is attributed to the transition O 1s to O 2p hybridized with cation sp orbitals. The modification from two-shell to eight-shell clusters is quite clear. Features B and C originate from medium-range effects. From the point of view of the scattering, these two spectral features come from outer-shell multiple scattering. The right panel presents larger-size O1 to O4 cluster calculations (eight-shell), showing the different behavior of the individual sites. All these calculated spectra show a very strong peak A because O atoms are bonded directly to Ti and Ba atoms. The higher intensity in the O1 spectrum reflects the shorter Ti—O1 distance, as expected.

In theory, one may calculate the partial density of states to further identify the origin of these spectral features. However, as mentioned above, band-structure calculations are not available for complex materials. In Fig. 4, as in one previous work on quartz (Wu et $al.$, 1998), we discuss a simplified cluster calculation (taking the O2 site as our example) using the first oxygen shell (curve a) only. Here the peak A disappears and the higher-energy part (above 10 eV from edge onset) becomes featureless. Curve (b) is a decomposed MS
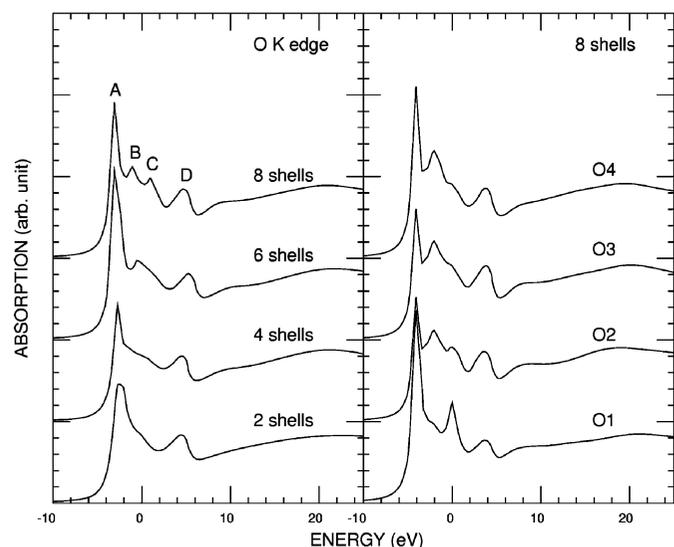
calculation of the two-shell cluster with the d bases of the bonded Ti and Ba atoms suppressed. Again, the pre-edge peak is not reproduced, but higher-energy features start to appear. This result is an additional demonstration that these higher-energy features are due to the hybridization between O 2p states and Ti and Ba sp states.

Curves (c) and (d) are the same cluster calculations with only one of the d bases of the Ba and Ti atoms, respectively, suppressed. Curves (c) and (d) confirm that feature A is associated mainly with the existence of unoccupied states of mixed O 2p orbitals and Ti 3d orbitals, while the B feature arises mainly from Ba d states.

Curve (e), the calculated spectrum of an O2-site two-shell cluster, is used for comparison. These calculations indicate an extensive spread in energy for O 2p orbitals and address a significant covalence in this compound (de Groot et $al.$, 1993).

4.2. Ba$_2$Ti$^{[5]}$Si$_2$O$_8$

Fresnoite, Ba$_2$Ti$^{[5]}$Si$_2$O$_8$, is a non-centrosymmetric tetragonal phase in space group $P4bm$. The structural features consist of Si$_2$O$_7$ groups linked to TiO$_5$ square pyramids, producing layers parallel to {001}. The barium cation, in tenfold coordination, connects the layers (Markgraf et $al.$, 1985). The unit cell contains four different O-atom sites (O1 to O4), which bond directly to two Si atoms for O1, one Si and three Ba atoms for O2, one atom each of Si, Ti and Ba for O3, and one Ti atom for O4. These different bonding configurations produce marked variations of the spectral features. The crystal data used for the MS calculations are based on single-crystal X-ray refinements (Masse et $al.$, 1967).

In Fig. 5, we present data for four individual clusters using larger atomic clusters (6 Å). All these spectra, as expected, are very different: the O1, O2 and O3 sites contribute mainly to peak E, which has basically the same origin as peak D in Ba$_2$TiO$_4$ but with a broad component arising from covalency between O and Si atoms. A weak peak A that appears in the O3 cluster calculation is associated with the hybridization of the Ti d orbital and O 2p states. The short and
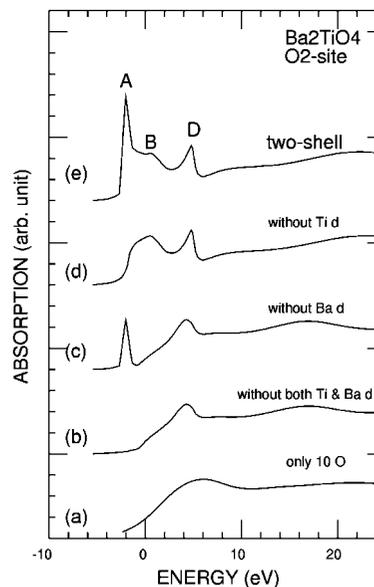
Figure 3
Left panel: theoretical MS calculations at the O K-edge as a function of the cluster size for Ba$_2$TiO$_4$ for clusters with increasing atomic shells: 2, 4, 6 and 8. The eight-shell cluster corresponds to a sphere of radius 6 Å. Right panel: MS calculations at the O K-edge for four individual O-atom sites using the eight-shell cluster.

Figure 4
MS calculations of the O K-edge ELNES in Ba$_2$TiO$_4$. (a) 10-O-atom only cluster calculation; (b) the decomposed calculation of a two-shell cluster taking O2 as the center, suppressing d bases of Ti and Ba; (c) the same as (b) but only suppressing Ba d bases; (d) the same as (b) but only suppressing the Ti d bases; (e) the normal two-shell cluster results.

single bond Ti—O4 leads to a direct interaction and overlap of their orbitals resulting in a strong peak A.

The sum of these four site contributions in the required proportion 1:2:4:1 produces the total calculated spectrum, which agrees well with the experimental one (Fig. 2).

4.3. CaTi$^{[6]}$SiO$_5$

In titanite, CaTi$^{[6]}$SiO$_5$, the primary structural units are corner-sharing TiO$_6$ octahedra running parallel to the *a* axis. Isolated SiO$_4$ tetrahedra share corners with these octahedra. Ca occupies an irregular seven-coordination polyhedron. The four O1 anions per unit cell are three-coordinated with two Ti atoms and one Ca atom. Each of the four O2 and O3 anions are three-coordinated with Si, Ti and Ca cations. The four O4 and O5 anions per unit cell are four-coordinated w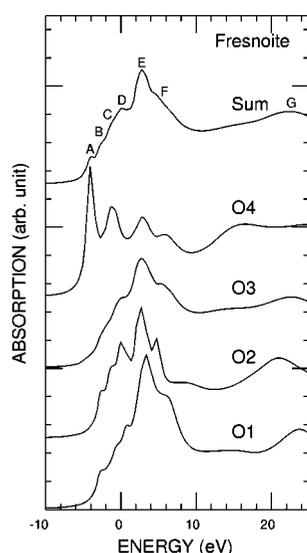ith one Si, one Ti and two Ca cations (Taylor & Brown, 1976). In Fig. 6 we only show the larger-size cluster calculations for five individual O atoms. Direct bonding of O1 to two Ti atoms with distances 1.76 Å and 1.98 Å, respectively, leads to a well resolved pre-edge peak A. Peak B originates from hybridization of O 2p and Ca 3d orbitals (see below). In order to understand the origin of this peak, we present in Fig. 7 a simplified 14-atom cluster calculation (from the O1 site), which contains the central O atom, its nearest two Ti atoms, one Ca atom and the outer shell with ten O atoms that provide an octahedral environment for these two Ti atoms. The doublet is well defined only in curves (*c*) and (*e*), while Ca only contributes to peak B (curve *d*). Therefore, the spectra also verify that this splitting is due to the local electrostatic interaction of the oxygen charges with the Ti *d* orbitals (*i.e.* the crystal field effect).

Coming back to Fig. 6, we underline that the O2–O5 site calculations are quite different from the O1 data. From the structural point of view, the immediate chemical environment of O1 does not contain Si atoms, *i.e.* there is no direct O1—Si bond that results in a lack of strong white-line peaks C and D. In Fig. 8, we verify this argument by taking a simplified 11-atom cluster around O2, which contains the central O atom, its nearest Si, Ti and Ca atoms, and an outer shell with seven O atoms. Curve (*a*) is almost the same as (*a*) in Fig. 7, since it is due to the contribution of the oxygen shell only. Conversely, comparison of curves (*b*)–(*d*) demonstrates that peaks C and D originate from the hybridization of O 2p with the nearest Si *s* and *p* bands.

4.4. (Ca,Sr,Ba)Ti$^{[6]}$O$_3$

CaTiO$_3$ has a distorted perovskite structure consisting of slightly deformed TiO$_6$ octahedra that are rotated relative to their positions in the ideal cubic phase. It has an orthorhombic cell with space group *Pbnm* (Buttner & Maslen, 1992; Beran *et al.*, 1996).

In Fig. 9, we report two individual O-atom-site calculations and their combination in the proportion 1:2 (curve *c*). A reasonably good agreement between experiment and theory was achieved, and all experimental features A–D are well reproduced, although the energy

Figure 5
MS calculations at the O *K*-edge for four individual O-atom sites in fresnoite using the eight-shell cluster and their sum in the proportion 1:2:4:1.
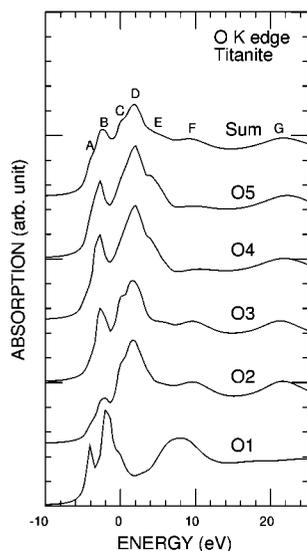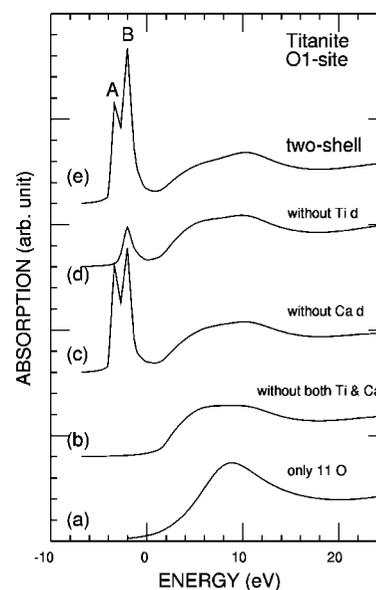
Figure 6
MS calculations at the O *K*-edge for five individual O-atom sites in titanite using the eight-shell cluster and their sum in the proportion 1:1:1:1:1.

Figure 7
MS calculations of the O *K*-edge ELNES in titanite taking O1 as the center of the cluster. (*a*) 11-O-atom only cluster calculation; (*b*) decomposed calculation of the two-shell cluster, suppressing the *d* bases of Ti and Ba; (*c*) the same as (*b*) but only suppressing the Ba *d* bases; (*d*) the same as (*b*) but only suppressing the Ti *d* bases; (*e*) the normal two-shell cluster results.

separation between features *A* and *C* is slightly smaller than the experimental value (Fig. 2).

Similar results for SrTiO$_3$ and BaTiO$_3$ are presented in Figs. 10 and 11, respectively. These perovskites have cubic symmetry (SrTiO$_3$, $Pm\bar{3}m$, with undistorted and unrotated TiO$_6$ octahedron) or tetragonal symmetry (BaTiO$_3$, $P4mm$), respectively. Structural data have been taken from single-crystal X-ray refinement (Hutton & Nelmes, 1981; Harada *et al.*, 1970).
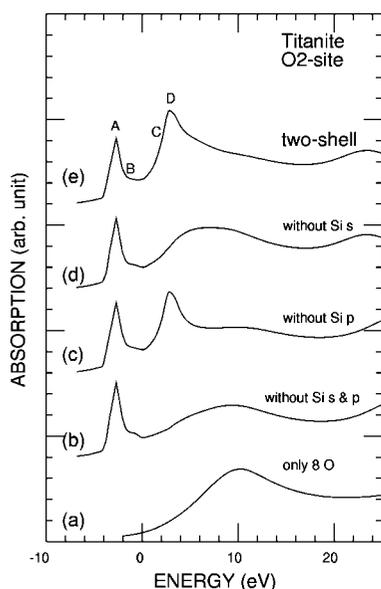

Figure 8
MS calculations of the O *K*-edge ELNES in titanite taking O2 as the center of the cluster. (*a*) 8-O-atom only cluster calculation; (*b*) the decomposed calculation of the two-shell cluster, suppressing the *sp* bases of Si; (*c*) the same as (*b*) but only suppressing the Si *p* bases; (*d*) the same as (*b*) but only suppressing the Si *s* bases; (*e*) the normal two-shell cluster results.
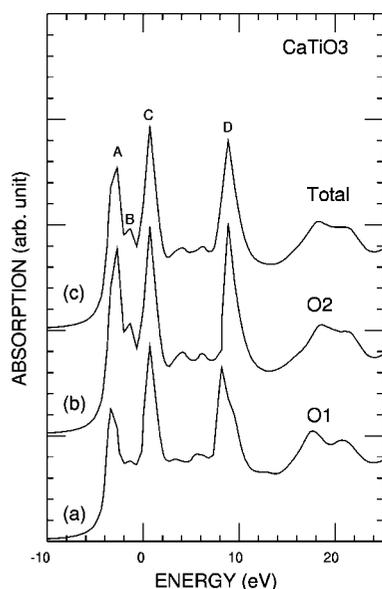

Figure 9
MS calculations at the O *K*-edge for two individual O-atom sites (*a* and *b*) and their sum (*c*) in the proportion 1:2 in perovskite CaTiO$_3$ using the eight-shell cluster.

In a previous work, de Groot *et al.* (1993) analyzed the O 1*s* X-ray absorption spectra of SrTiO$_3$ using the localized spherical-wave method with an extended basis set to describe the unoccupied states over a wider energy range. However, in their work the calculated density of states for SrTiO$_3$ is in disagreement with experiment, not only in the pre-edge but also in the higher-energy region. They attributed this disagreement to the core-hole potential, but we cannot exclude the possibility of wrong Wyckoff position for both O and S atoms [see Table I of de Groot *et al.* (1993)]. From our decomposed MS calculation for BaTiO$_3$ (see Fig. 12) taking the O2-site cluster, we find that all pre-edge peaks disappear when the *d* orbitals of the nearest Ti and Ba atoms (curve *a*) are suppressed. When suppressing the Ba *d* orbitals only, the pre-edge peak *A* remains, indicating that it is mainly due to the Ti *d* contribution (curve *b*). Peak *B* is due to the superimposition of Ti and Ba, while *C* mainly originates from the Ba *d* bands [curves (*c*) and (*d*)] in agreement with the band-structure calculation (de Groot *et al.*, 1993).

In all the spectra of these three perovskites *X*TiO$_3$ (*X* = Ca, Sr and Ba) (Fig. 1), a chemical shift of the first peak is not observed, contrary to the observation of Soriano *et al.* (1993) for the *d*^{0} oxides of the group IV*a* and V*a* elements, because in these perovskites the states in the unoccupied bands just above the Fermi level have most weight on the Ti sites.

However, the chemical shift of the first peak is also not observed in alkaline-earth oxides (Nakai *et al.*, 1987).

4.5. Core-hole potential

Finally, we present in Fig. 13 a comparison between the fully relaxed final-state (*Z* + 1 approximation) and the ground-state (GS) potential calculations. The results are quite similar for the two different potential calculations, except for a minor difference in the relative intensities of the pre-edge features. This is because the core hole is now located on the O-atom site while the states in the unoccupied bands just above the Fermi level have most weight on the cation site.
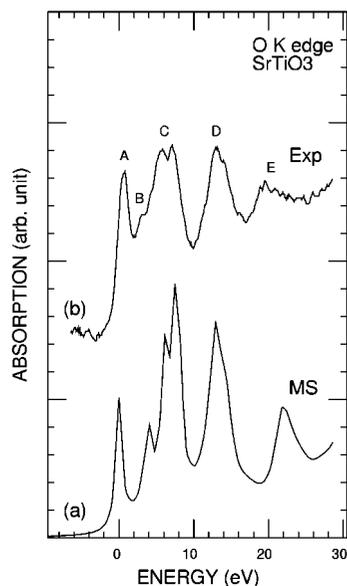

Figure 10
MS calculations at the O *K*-edge in perovskite SrTiO$_3$ using the eight-shell cluster, along with the experimental spectrum.

5. Conclusion

We have carried out experimental and theoretical investigations of O K-edge ELNES spectra of Ti-bearing compounds Ba_2TiO_4, $Ba_2TiSi_2O_8$ (fresnoite), $CaTiSiO_5$ (titanite), and perovskites $XTiO_3$ with X = Ca, Sr and Ba. Good agreement between experimental data and MS calculations has been achieved. Moreover, the MS decomposed analysis offers the direct possibility for these complex compounds to extract the respective atomic and electronic structures in terms of partial and local band contributions. The variations in shape and intensity of the peaks have also been analyzed in terms of the first-nearest cation atoms or Si and the bond length. Actually, the features present in the first several eV above the edge onset are a
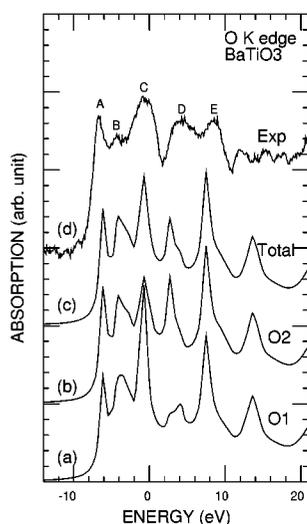

Figure 11
MS calculations at the O K-edge for two individual O-atom sites and their sum in the proportion 1:2 in perovskite $BaTiO_3$ using the eight-shell cluster, along with the experimental spectrum.
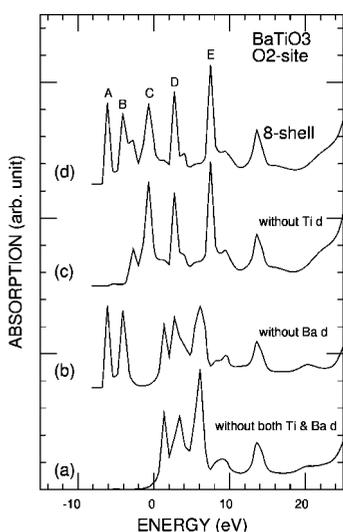

Figure 12
MS calculations of the O K-edge spectra in $BaTiO_3$. (a) The decomposed calculation of the eight-shell cluster taking O2 as the center but suppressing the d bases of Ti and Ba; (b) the same as (a) but only suppressing the Ba d bases; (c) the same as (a) but only suppressing the Ti d bases; (d) the normal eight-shell cluster results (without convolution).

fingerprint of the electronic structure of the cation in the local crystal field. They are related to the lowest-energy states in the unoccupied conduction band.

To conclude, we may underline that the shape of the pre-edge peaks is strongly correlated with the first cation atoms (Ti and/or other metals) and their crystal field (tetrahedral, pentahedral or octahedral field), whereas the intensity of the pre-edge peaks appears to be determined by the local structural environment, *i.e.* bond length and coordination number. As demonstrated by MS decomposed calculations, the Ba_2TiO_4 spectrum is characterized in the pre-edge region by the short-range interaction between $Ti^{[4]}$ and Ba d with O $2p$ states. In fresnoite and titanite, the nearest Si atoms influence this hybridization process between the central O and Ti and/or other cations leading to weak poorly resolved pre-edge peaks. For perovskites, the alkaline-earth elements (Ca, Sr and Ba) play an important role, and they are strongly related to a peak at about 8 eV in these spectra.

In principle, all features of O K-edge spectra above 539 eV can be identified using the decomposed MS analysis and shell-by-shell results, even if the structure is complex. These features essentially reflect the mean-range order. The quality of our simulations is well demonstrated by comparison with the experimental data. However, to be more effective we performed simulations also with other potentials. These investigations also demonstrate that the core-hole potential is not adequate, especially for $XTiO_3$ (X = Ca, Sr and Ba) compounds, as shown by the comparison between the $Z + 1$ approximation and the ground-state (GS) potential.
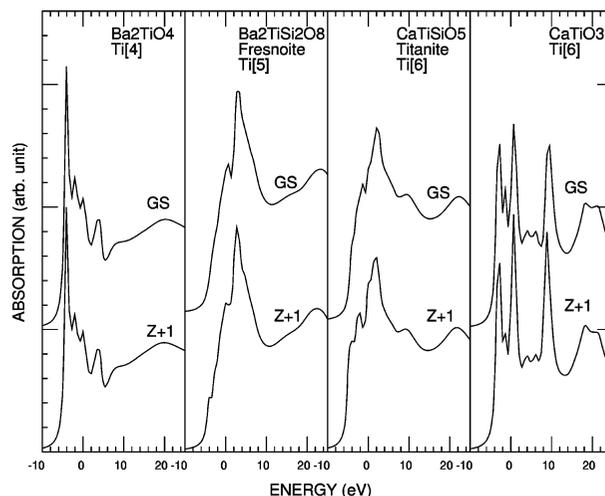
Figure 13
Comparison between two MS calculations at the O K-edge for Ba_2TiO_4, fresnoite ($Ba_2TiSi_2O_8$), titanite ($CaTiSiO_5$) and perovskite $CaTiO_3$, made using two different final-state potentials: the $Z + 1$ final-state potential (lower curve) and the ground-state (GS) potential (upper curve).

research papers

References

Aken, P. A. van, Liebscher, B. & Styrsa, V. J. (1998*a*). *Phys. Chem. Miner.* **25**, 494–498.

Aken, P. A. van, Liebscher, B. & Styrsa, V. J. (1998*b*). *Phys. Chem. Miner.* **25**, 323–327.

Aken, P. A. van, Wu, Z. Y., Langenhorst, F. & Seifert, F. (1999). *Phys. Rev. B*, **60**, 3815–3820.

Beran, A., Libowitzky, E. & Armbruster, T. (1996). *Can. Mineral.* **34**, 803–809.

Brydson, R., Sauer, H. & Engel, W. (1992). *Transmission Electron Energy Loss Spectroscopy in Materials Science*, edited by M. M. Disko, C. C. Ahn & B. Fultz, pp. 131–154. Warrendale, PA: TMS.

Buttner, R. H. & Maslen, E. N. (1992). *Acta Cryst.* B**48**, 644–649.

Cabaret, D., Sainctavit, P., Ildefonse, P. & Flank, A.-M. (1998). *Am. Mineral.* **83**, 300–304.

Clementi, E. & Roetti, C. (1974). *Atom. Data Nucl. Data Tables*, **14**, 177.

Durham, P. J. (1988). *X-ray Absorption: Principles, Applications, Techniques of EXAFS, SEXAFS, XANES*, edited by R. Prinz & D. Koningsberger. New York: Wiley.

Egerton, R. F. (1996). *Electron Energy-Loss Spectroscopy in Electron Microscopy*, pp. 485. New York: Plenum Press.

Garvie, L. A. J. & Buseck, P. R. (1998). *Nature* (*London*), **396**, 667–670.

Garvie, L. A. J. & Craven, A. L. (1994). *Phys. Chem. Miner.* **21**, 191–206.

Gibbs, G. V., Downs, J. W. & Boisen, M. B. Jr (1994). *Silica, Physical Behavior, Geochemistry and Materials Applications*, edited by P. J. Heaney, C. T. Prewitt & G. V. Gibbs, *Reviews in Mineralogy 25*, pp. 331–368. Washington, DC: Mineralogical Society of America.

Groot, F. M. F. de, Faber, J., Michiels, J. J. M., Czyzyk, M. T., Abbate, M. & Fuggle, J. C. (1993). *Phys. Rev. B*, **48**, 2074–2080.

Groot, F. M. F. de, Grioni, M., Fuggle, J. C., Ghijsen, J., Sawatzky, G. A. & Petersen, H. (1989). *Phys. Rev. B*, **40**, 5715–5723.

Harada, J., Pedersen, T. & Barnea, Z. (1970). *Acta Cryst.* A**26**, 336–344.

Hutton, J. & Nelmes, R. J. (1981). *Acta Cryst.* A**37**, 916–920.

Jollet, F., Petit, T., Gota, S., Thromat, N., Gautier-Soyer, M. & Pasturel, A. (1997). *J. Phys. Condens. Matter*, **9**, 9393–9400.

Kurata, H., Lefevre, E., Colliex, C. & Brydson, R. (1993). *Phys. Rev. B*, **47**, 13763–13768.

Lee, P. A. & Beni, G. (1977). *Phys. Rev. B*, **15**, 2862–2883.

Lee, P. A. & Pendry, J. B. (1975). *Phys. Rev. B*, **11**, 2795–2811.

Markgraf, S. A., Halliyal, A., Bhalla, A. S., Newnham, R. E. & Prewitt, C. T. (1985). *Ferroelectrics*, **62**, 17–26.

Masse, R., Grenier, J. C. & Durif, A. (1967). *Bull. Soc. Fran. Mineral. Cristall.* **90**, 20–23.

Mattheiss, L. (1964). *Phys. Rev. A*, **134**, 970–973.

Nakai, S., Mitsuishi, T., Sugawara, H., Maezawa, H., Matsukawa, T., Mitani, S., Yamasaki, K. & Fujikawa, T. (1987). *Phys. Rev. B*, **36**, 9241–9246.

Natoli, C. R. & Benfatto, M. (1986). *J. Phys. Paris Colloq.* **47**, C8–11–23.

Natoli, C. R., Benfatto, M., Brouder, C., Ruiz Lopez, M. Z. & Foulis, D. L. (1990). *Phys. Rev. B*, **42**, 1944–1962.

Natoli, C. R., Benfatto, M. & Doniach, S. (1986). *Phys. Rev. B*, **34**, 4682–4694.

Natoli, C. R., Misemer, D. K., Doniach, S. & Kutzler, F. W. (1980). *Phys. Rev. A*, **22**, 1104–1108.

Norman, J. G. Jr (1974). *Mol. Phys.* **81**, 1191–1203.

Penn, D. R. (1987). *Phys. Rev. B*, **35**, 482–486.

Soldatov, A.V., Kasrai, M. & Bancroft, G. M. (2000). *Solid State Commun.* **115**, 687–692.

Soriano, L., Abbate, M., Fuggle, J. C., Jimenez, M. A., Sanz, J. M., Mythen, C. & Padmore, H. A. (1993). *Solid State Commun.* **87**, 699–705.

Stöhr, J. (1988). *X-ray Absorption: Principles, Applications, Techniques of EXAFS, SEXAFS, XANES*, edited by R. Prinz & D. Koningsberger. New York: Wiley.

Taylor, M. & Brown, G. E. (1976). *Am. Mineral.* **61**, 435–447.

Wu, K. K. & Brown, I. D. (1973). *Acta Cryst.* B**29**, 2009–2012.

Wu, Z. Y., Jollet, F. & Seifert, F. (1998). *J. Phys. Condens. Matter*, **10**, 8083–8089.

Wu, Z. Y., Marcelli, A., Mottana, A., Giuli, G. & Paris, E. (1997). *Europhys. Lett.* **38**, 465–470.

Wu, Z. Y., Ouvrard, G., Gressier, P. & Natoli, C. R. (1997). *Phys. Rev. B*, **55**, 10382–10391.

Yoshiya, M., Tanaka, I., Kaneko, K. & Adachi, H. (1999). *J. Phys. Condens. Matter*, **11**, 3217–3221.